Macromolecules

ARTICLE

pubs.acs.org/Macromolecules

In Situ Synchrotron X-ray Scattering Study on Isotactic Polypropylene Crystallization under the Coexistence of Shear Flow and Carbon Nanotubes

Yan-Hui Chen,[†] Gan-Ji Zhong,[†] Jun Lei,[†] Zhong-Ming Li,[*,†] and Benjamin S. Hsiao[*,‡]

[†]College of Polymer Science and Engineering and State Key Laboratory of Polymer Materials Engineering, Sichuan University, Chengdu 610065, China

[‡]Department of Chemistry, Stony Brook University, Stony Brook, New York 11794-3400, United States

Supporting Information

ABSTRACT: The crystallization of isotactic polypropylene (iPP) under the coexistence of shear flow and carbon nanotubes (CNTs) was investigated by means of in situ synchrotron X-ray scattering techniques, i.e. wide-angle X-ray diffraction (WAXD) and small-angle X-ray scattering (SAXS). Compared to sheared pure iPP, the combined effect of shear flow and CNTs endowed iPP crystals with weak degree of orientation at the early stage of crystallization but high degree of orientation in the later period. This was because the initial orientation of molecular chains induced by shear was suppressed as a result of the increased viscoelasticity of iPP melt in the presence of CNTs, but subsequently oriented molecular chains were stabilized by CNT surface absorption. The crystallization kinetics of sheared CNTs/iPP nanocomposites was synergistically promoted, where the crystallization rate was increased about 40 times in comparison to that of quiescently crystallized pure iPP. The Avrami exponent of CNTs/iPP nanocomposites and sheared iPP was around 2, indicating two-dimensional lamellar growth. The Avrami exponent of sheared CNTs/iPP nanocomposites surprisingly appeared to be 2.52, suggestive of mixed two-dimensional lamellar growth and three-dimensional sphrulitic growth geometries. Moreover, β-crystals were absent in sheared CNTs/iPP nanocomposites in contrast to the normal observation that α-row nuclei induced by shear generated β-crystals. The synergistic crystallization rate, the mixed crystal growth geometry as well as the absence of β-crystals in sheared CNTs/iPP nanocomposites were in close relation with intense interaction between shear flow and CNTs, which gave rise to extra nuclei in sheared CNTs/iPP melt. Apart from heterogeneous nucleating sites originated from CNTs and homogeneous nucleating sites (row-nuclei) initiated by shear, extra nuclei were taken into account to contribute to the further accelerated crystallization kinetics. The extra nuclei became active growth points of branching sites on the two-dimensional lamellae to generate three-dimensional spherulitic growth, thus leading to mixed crystal growth geometry of sheared CNTs/iPP nanocomposites. Besides, extra nuclei as well as α-nuclei derived from CNTs remarkably encouraged the formation of α-crystals, responsible for inexistence of β-crystals in sheared CNTs/iPP nanocomposites.

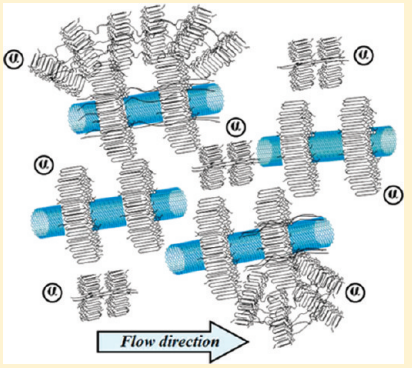

INTRODUCTION

Carbon nanotubes (CNTs), which possess high flexibility, low mass density, and large aspect ratio,[1] have been well proved to exhibit the potential to offer extraordinary mechanical, electrical and thermal properties to polymeric materials.[2−5] By providing sufficient heterogeneous nucleation sites, CNTs could remarkably suppress the energy barrier for polymer crystallization,[6] thus acting as an effective nucleating agent for various semicrystalline polymers such as polyethylene (PE), isotactic polypropylene (iPP), and poly(ethylene terephthalate). The addition of CNTs to polymers can considerably accelerate crystallization kinetics,[7−11] and alter crystalline morphology.[11−16] For instance, the poly(ethylene terephthalate) nanocomposites containing single wall carbon nanotubes (SWNTs) at a concentration as low as 0.03 wt % crystallized 10 °C earlier than the nascent poly(ethylene terephthalate).[10] The addition of 1 wt % SWNTs reduced the half crystallization time ($t_{1/2}$) to just 7% of $t_{1/2}$ of the pure PE when isothermally crystallized at 122 °C.[11] On the other hand, CNTs have been well accepted to be able to absorb polymer molecular chains to their surface and subsequently template crystal growth, resulting in special crystalline morphology through appropriate lattice matching.[13−16] A typical and delicate morphology is the "nano-hybrid shish-kebabs" (NHSK) structure directly observed by Li et al., where CNTs serve as shish and disk-shaped polymer single crystals (kebabs) grow periodically epitaxially perpendicular to the surface of CNTs, obeying "size-dependent soft epitaxy" formation mechanism.[13,14] The Avrami equation as a semiempirical expression is widely applied to indirectly characterize the

Received: July 22, 2011
Revised: September 1, 2011
Published: September 16, 2011

dimensionality of growth in CNTs-induced polymer crystallization, where the Avrami exponent, *n*, ranges from 1 to 4 and broadly describes dimensionality as the regions from 1 to 2, 2 to 3, and 3 to 4, corresponding to one-, two-, and three-dimensional growth, respectively. Winey et al. indicated that SWNTs reduced the crystal dimensionality from spherulitic to disk-shaped with Avrami exponent *n* approximately equal to 1.6 for the HDPE composites with 1 wt % SWNTs.[11] Kaminsky et al. put forward that the dimensionality of the Avrami parameter ranged from 2 to 2.8 changing from a disk-like growth with instantaneous nucleation to a random nucleation or from a rod-like to a more disk-like growth (with random nucleation) in CNTs/iPP system.[17] Others argued that the Avrami exponent close to 3 implied a three-dimensional heterogeneous crystal growth and was practically unchanged with the addition of CNTs to iPP.[7−9] The Avrami exponent of CNTs-induced polymer crystallization has been discussed controversially since it is intimately related to the concentration, dispersion state and aspect ratio of CNTs, crystallization and processing conditions, etc.

Analogous to CNTs-induced polymer crystallization, shear flow, which inevitably exists in common polymer processing operations (e.g., extrusion, injection and blowing molding), has been also well proved to drastically influence crystallization kinetics[18−22] and crystalline morphology of semicrystalline polymers.[23−27] Through reducing the entropy of polymer molecular chains,[28] the shear flow induced oriented nuclei in a lower free energy, thus enhancing the crystallization process.[29,30] In general, polymer molecular chains with a coiled conformation might undergo a coil-to-stretch transition upon an extension/shear flow,[31,32] where those stretched polymer molecular chains higher than a critical molecular weight (M^*) aggregated to form extended chain fibrils, and afterward the remaining coiled chains could crystallize upon the fibrils in a folded periodic fashion,[33] finally forming the shish-kebab morphology, which can profoundly improve the ultimate properties of shaped products.[26,34−36] Avrami equation was also employed to evaluate the crystal geometry, the nucleation type and the nature of crystal growth in flow-induced polymer crystallization system.[37−41] Strictly speaking, Avrami equation used in this way is only true for successive crystallization occurring under isothermal condition after a brief shear pulse. Hsiao et al. strongly supported that after step shear the growth of oriented PP crystals belonged to a rod or disk-like crystal growth geometry with the value of Avrami exponent, *n*, ranging from 1.8 to 2.8.[38,39]

It has to be noted that most of the studies on flow-induced crystallization have been carried out on relatively neat polymers. However, in reality, an additive package (nucleating agents, fibers, particles, and CNTs etc.) was frequently added to polymers in order to achieve high-performance and multifunctional polymers.[42−45] Under quiescent condition, the final crystalline structure and morphology are determined by the additive characteristics (such as concentration, composition, additive size, and shape) and by the interaction between the additives and the polymer. When shear flow is present, the influencing effects extend to shear rate, shear duration, the interaction between shear and additives, etc. Since the coexistence of shear flow and additives makes the crystallization process a little complicated, the combined effect of both factors on the crystallization of polymers has not yet been studied comprehensively so far. It is certain that a profound influence of the coexistence of shear flow and additives on structure evolution and final properties of products can be expected. Both factors are prone to increase nucleation sites, which in turn encourage the crystallization kinetics. Hence, the contribution of both factors relative to each other is believed to be of importance. Early study by Lagasse et al.,[46] later study by Naudy et al.,[47] and recent study by D'Haese et al.[48] reported that the acceleration of the crystallization kinetics with the increasing shear rate was less remarkable for polymers containing nucleating agents or particles. These authors concluded that the contribution of nucleating agents or particles and shear flow to nucleation density was additive: at low shear rates the contribution of nucleating agent or particles dominated; at higher shear rates the shear flow became more significant. As investigated by other studies, the relative contribution of shear flow and additives to the crystallization process was considered differently to be resulted from a specific interaction or synergy between the additives and the surrounding polymer matrix. For example, Larin et al., through comparing the combined contribution of aramid fibers and shear flow with individual contributions of aramid fibers and shear flow, definitely believed that the combined effect was synergistic rather than simple additive in sheared aramid fibers filled iPP system.[49] Our recent study on graphene nanosheets and shear flow-induced crystallization in iPP nanocomposites also suggested that the presence of graphene nanosheets and shear flow exhibited a synergistic interaction on promoting crystallization kinetics of iPP, although it was not markedly dependent on the concentration of graphene nanosheets.[50] Extra nucleation sites created by the strong interaction between nucleating agents and flow fields were proposed by Byelov et al.[51] and our group,[52] and the number was further calculated in a semiquantitative way. Many authors have contributed the synergy between additives and matrix to the changes in the local stress levels and orientation of the polymer molecular chains surrounding an additive upon the application of shear.[50,53,54] As for CNTs/polymer nanocomposites, it has not been clear whether the combined effect of shear flow and CNTs on crystallization kinetics is additive or synergistic.

The resultant crystal orientation is affected by the combined effect of shear flow and additives as well. Janeschitz-Kriegl et al. proposed a nucleation mechanism that additives served as point nuclei on which polymer molecular chains could be absorbed and subsequently be stretched along the flow fields to form thread-like precursors.[55,56] Additionally, due to the adsorption of additive surfaces[57,58] or the network interconnected by additives,[59] the precursors can be stabilized to form oriented structure rather than relaxed. This is able to explain why in filled polymers crystallized after duct flow orientation is enhanced as compared to pure polymers. This enhanced orientation can be observed in almost all studies concerning the effect of flow fields on filled polymers,[49,50,59−61] especially in the case of polymer nanocomposite system with well-dispersed, one-dimensional and anisotropic CNTs.[57,58,62,63] For example, García-Gutiérrez et al. stated that both poly(butylene terephthalate) chains and CNTs were arranged in the flow direction, and CNTs bundles tended to template polymer lamellae to grow perpendicularly to the CNTs surfaces in a shish-kebab-like fashion.[57] Moreover, they also proposed that the effect of CNTs was to counterbalance nuclei relaxation by providing surfaces. Systematic studies were performed on sheared CNTs/PE nanocomposites by Rastogi et al.[58,62,63] They concluded that upon shear flow the presence of CNTs was favorable for the increase of shish length and chain orientation as well as stabilization of shish, apart from the accelerated polymer crystallization kinetics, due to the strong chain-nanotube interactions. Hence, the stabilization of CNTs to oriented molecular chains was identified. However, when CNTs/polymer melt suddenly encounters a shear flow, the initial response of the

melt is still vague. As aforementioned, Avrami equation was extensively adopted to describe the dimensionality of crystal growth. To our best of knowledge, Avrami equation was barely used in sheared CNTs/polymer nanocomposites, except one case conducted by Mago et al. that unexpectedly and significantly high (6.5−8.0) values of n were calculated by an Avrami-type equation for the normalized storage modulus in sheared CNTs/poly(butylene terephthalate) nanocomposites.[64]

iPP is one of the most important thermoplastic polymers in industry, which is ascribed to its low manufacturing cost and versatile properties. Meanwhile, iPP demonstrates interesting polymorphic behaviors, depending on the polymerization procedure, thermal history, and use of different nucleating agents.[42,52,65] Research on CNTs/iPP nanocomposites under shear flow are of great importance. In this work, the crystallization behavior of CNTs/iPP nanocomposites with a small amount of CNTs (0.1 wt %) after step shear was characterized by in situ synchrotron wide-angle X-ray diffraction (WAXD) and small-angle X-ray scattering (SAXS) techniques. The shear-induced crystallization behavior and polymorphism of iPP nanocomposites have been intensively investigated, which enables us to better understand the combined effect of shear flow and CNTs on the crystallization kinetics, crystal growth as well as evolution of crystal orientation structure.

EXPERIMENTAL SECTION

Materials. iPP, model T30S, was purchased from Dushanzi Petroleum Chemical Co., China, with a melt flow rate (MFR) of 3 g/10 min (230 °C, 21.6 N), $M_w = 39.9 \times 10^4$ g mol^{-1}, and $M_w/M_n = 4.6$. Multiwalled CNTs of outer diameter (o.d.) 30−50 nm and length 10−20 μm were purchased from Chengdu Organic Chemicals Co., Ltd., the Chinese Academy of Sciences R&D Center for Carbon Nanotubes. Anhydrous ethanol (AR grade) and xylene (AR grade) were purchased from Chengdu Kelong Chemical Reagent Factory (China) and were used as received.

Sample Preparation. Solution blending method was utilized to prepare the iPP nanocomposite with 0.1 wt % CNT content. The detailed preparation procedure was as follows: iPP (10 g) was dissolved in xylene (100 mL) at 140 °C by continuous stirring in an oil bath for 2 h. CNTs (10 mg) were dispersed in anhydrous ethanol (100 mL) and sonicated for 15 min to obtain a uniform dispersion. Then the mixture was coagulated by adding anhydrous ethanol/CNTs suspension into xylene/iPP hybrid with continuous stirring. Thereafter, the mixture was transferred to evaporating dishes, left overnight at room temperature, and dried in a vacuum oven for 2 days at 80 °C to evaporate the residual solvent. The films with 0.5 mm thick were obtained by compression molding the mixture at 200 °C for 5 min under a pressure of 10 MPa. Good dispersion of CNTs can be observed in Supporting Information. For concision, iPP nanocomposite with 0.1 wt % CNTs was defined as iPP01, while neat iPP as iPP0.

X-ray Measurements. WAXD and SAXS measurements were carried out at the Advanced Polymers Beamline (X27C, λ = 0.1371 nm) in the National Synchrotron Light Source (NSLS), Brookhaven National Laboratory (BNL). A 2D MAR CCD X-ray detector (MARUSA) was employed for detection of 2D-WXAD and 2D-SAXS images, having a resolution of 1024 × 1024 pixels (pixel size =158.44 μm). The data acquisition time was 30 s for each scattering pattern (image). The sample to detector distance was 112.6 mm and 2330 mm for WAXD (calibrated by an aluminum oxide (Al_2O_3) standard) and SAXS (calibrated by a silver behenate (AgBe) standard), respectively. The scattered intensities were registered in the range of scattering angles 2θ from 10 to 30°.

Linear WAXD profiles were obtained from circularly integrated intensities of 2D-WAXD image patterns acquired, applied to linear SAXS as well. The intensity was plotted as a function of the scattering vector, q, where $|q| = 4\pi(\sin\theta)/\lambda$, λ is the wavelength of the incident beam, and 2θ is the scattering angle. Subsequently, through deconvoluting the peaks of linear WAXD profiles, the overall crystallinity X_c was calculated by

$$X_c = \frac{\sum A_{cryst}}{\sum A_{cryst} + \sum A_{amorp}} \quad (1)$$

where A_{cryst} and A_{amorp} are the fitted areas of crystal and amorphous, separately. The normalized relative crystallinity (X_r) was used to estimate crystallization kinetics of neat iPP and its nanocomposites, by means of the following equation:

$$X_r = \frac{X_c(t)}{X_c(\infty)} \quad (2)$$

where X_r is normalized relative crystallinity of iPP, and $X_c(t)$ and $X_c(\infty)$ are the fitting crystallinity of iPP at holding time (t) and completion of crystallization, respectively.

Herman's method was used to determine the degree of orientation of lamellae crystals in the sheared melt.[66] Accordingly, the crystalline orientation can be characterized by the average orientation of the normal to the crystalline plane with respect to an external reference frame. Here, the flow direction was taken as the reference direction. For a set of hkl planes, the average orientation, expressed as $\langle\cos^2\phi\rangle_{hkl}$, can be calculated mathematically using the following equation:

$$\langle\cos^2\phi\rangle_{hkl} = \frac{\int_0^{\pi/2} I(\phi)\cos^2\phi\sin\phi\,d\phi}{\int_0^{\pi/2} I(\phi)\sin\phi\,d\phi} \quad (3)$$

where ϕ is the azimuthal angle and $I(\phi)$ is the scattered intensity along the angle ϕ. Herman's orientation function, f, can be defined as

$$f = \frac{3\langle\cos^2\phi\rangle_{hkl} - 1}{2} \quad (4)$$

where f has a value of −0.5 when the normal of the reflection plane is perpendicular to the reference direction (ϕ = 90°), a value of 1 when normal of the reflection plane parallel is the reference direction (ϕ = 0°), and a value of 0 when the orientation are random. For evaluation of the degree of orientation, the azimuthal intensity distribution $I(\phi)$ at q = 1.20 is analyzed. This peak represents the (040) reflection of α-crystals in iPP, which only appears at the equator in the WAXD patterns once oriented. The value of f ranges from 0 to 1, due to the diffraction characteristics of (040) lattice plane, where the value of f increases from 0 to 1, illustrating that crystal reflection plane changes from random distribution to alignment along flow direction.

Experimental Procedures. A Linkam CSS-450 high-temperature shearing stage modified for in situ synchrotron X-ray scattering studies was used to precisely control shear flow field and thermal history of the polymer samples. The temperature protocol and shear conditions used during the WAXD and SAXS experiments are shown in Figure 1. The experimental temperature profiles of isothermal crystallization in Figure 1a were set as

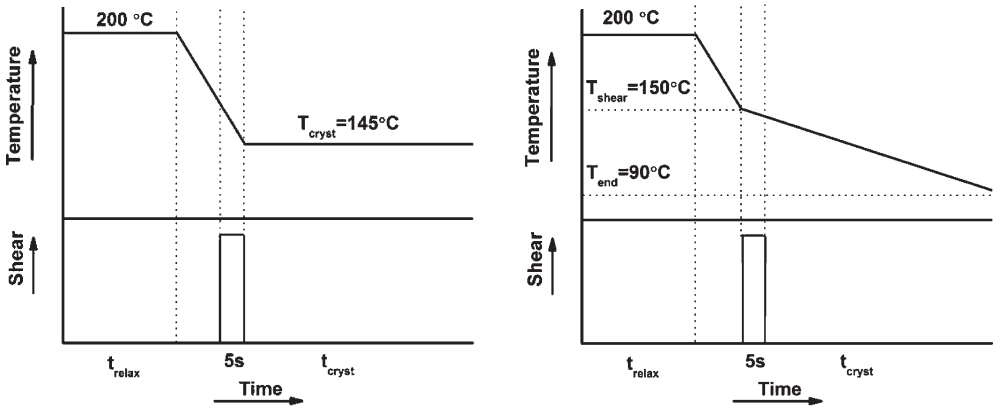

Figure 1. Schematics of the temperature and shear conditions (step shear 20 s^{-1} for 5 s) as a function of time for WAXD and SAXS experiments: (a) isothermal crystallization and (b) nonisothermal crystallization.

follows: (1) heating at a rate of 30 °C/min from room temperature to 200 °C; (2) holding the temperature at 200 °C for 5 min to eliminate residual structure; (3) cooling at a rate of 30 °C/min down to 145 °C; (4) holding the temperature at 145 °C for enough time until the crystallization finished for X-ray measurements. The experimental temperature profiles of nonisothermal crystallization in Figure 1b were set as follows: (1) heating at a rate of 30 °C/min from room temperature to 200 °C; (2) holding the temperature at 200 °C for 5 min to eliminate residual structure; (3) cooling at a rate of 30 °C/min down to 150 °C; (4) then, cooling at a rate of 2 °C/min down to 90 °C, which took about 30 min for X-ray measurements. The applied shear rate was 20 s^{-1} with the duration of 5s.

RESULTS

Isothermal Crystallization under Quiescent Conditions. Some studies utilized a differential scanning calorimeter, a rheometer, etc. to reveal the high CNT nucleation efficiency in iPP under quiescent condition.[7−11] The CNT dosage normally ranged from 0.03 to 30 wt %, but generally exceeded 0.1 wt %. To compare with the results obtained by DSC, isothermal crystallization of CNTs/iPP nanocomposites under quiescent condition was probed by in situ synchrotron X-ray scattering. Here, a quite low CNT loading, 0.1 wt %, was added. Figure 2 shows a representative series of 2D-WAXD images during isothermal crystallization of iPP0 and iPP01 samples at 145 °C under quiescent condition. No crystal reflections are observed in the first pattern (t = 0 min) of iPP0 and iPP01, confirming that the crystal structure of iPP has been completely erased off before cooled to crystallization temperature. The characteristic lattice planes of α-crystals in both samples, i.e. (110), (040), (130), (111), and (−131), from inner to outer, are developing homogeneously (Figure 2b,c) until the completion of crystallization (Figure 2d). The time evolution of linear WAXD curves of iPP0 and iPP01 is then shown in Figure 3. Both samples share the same crystal growth process: the appearance and successive development of α-crystals, while the induction and completion time of iPP01 decreases from 23 and 248 min of iPP0 to 6 and 51 min, respectively. This indicates that the small amount addition of CNTs (only 0.1 wt %) can accelerate the crystallization rate remarkably. In the Supporting Information, it can be found that 0.1 wt % CNT loading gives rise to 10 °C

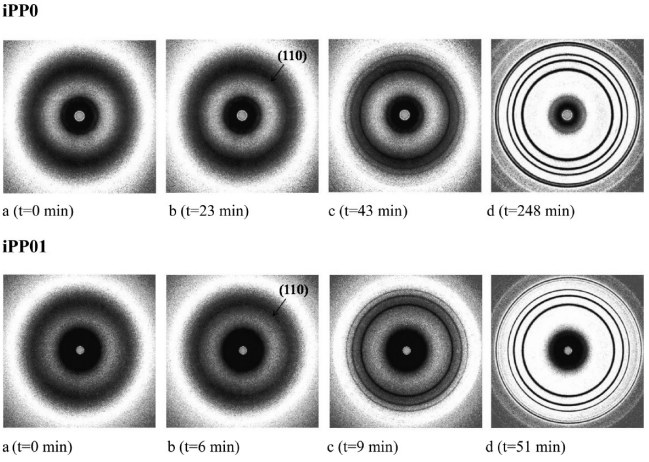

Figure 2. Selected 2D-WAXD patterns showing the crystal growth process of pure iPP (iPP0) and iPP with 0.1 wt % CNTs (iPP01) isothermally crystallized at 145 °C under quiescent condition.

increase of iPP peak crystallization temperature under nonisothermal crystallization process via DSC measurement, compared to pure iPP. The same increase of crystallization temperature was also observed by Miltner et al. But the CNT loading was increased to 2 wt %.[67] This illustrates the acceleration of the crystallization saturates with the increasing of CNT content, where 0.1 wt % CNT may be the saturated content.

Isothermal Crystallization under Shear. To reveal the combined effect of shear and CNTs on the crystal evolution during isothermal crystallization of iPP, selected 2D-WAXD patterns of iPP0 and iPP01 isothermally crystallized at 145 °C after step shear are shown in Figure 4. The initial images of both samples in Figure 4 show diffuse scattering, even though the melt may be oriented, possibly due to the detection limitation of the WAXD technique.[52] Surprisingly, there are no obvious arc-like diffraction intensities appeared in the whole crystallization process of sheared iPP0 (Figure 4b−d). In contrast to sheared iPP0, obvious arc-like diffraction feature of α-crystal (040) crystal plane along the meridian is clearly observed in sheared iPP01 (Figure 4b−d). These oriented crystals are formed under the combined effect of shear and CNTs, in other words, crystal

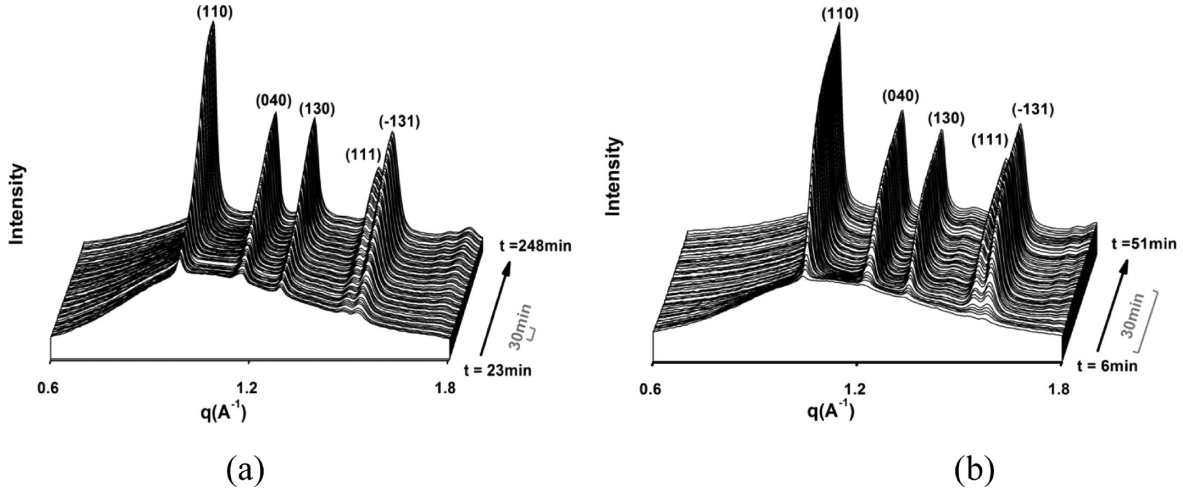

Figure 3. Linear WAXD intensity profiles of (a) iPP0 and (b) iPP01 quiescently crystallized at 145 °C as a function of scattering sector, q, of iPP melt, obtained from circularly integrated intensities of 2D-WAXD patterns in Figure 2.

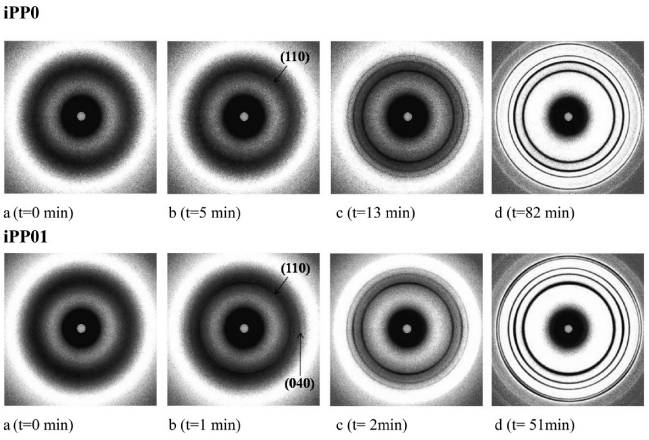

Figure 4. Selected 2D-WAXD patterns of iPP0 and iPP01 showing the crystal growth process of iPP isothermally crystallized at 145 °C after step shear. The shear direction is vertical.

orientation is enhanced by the addition of CNTs under shear. Generally, only polymer molecules above the "critical orientation molecular weight" (M^*) could remain oriented after shear at a given shear rate ($\dot{\gamma}$), following the relationship $M^* \propto \dot{\gamma}^{-\alpha}$ where α is a positive exponent.[32] The memory of the flow field will be erased if the sheared sample is kept quiescently at a high temperature for a sufficient long time. This is because the shear-induced oriented precursors are intrinsically unstable at high temperatures.[40,68] Considering the case of sheared iPP0, after the relatively weak shear flow ($20\ s^{-1}$ for 5 s) the sample was crystallized at a low degree of supercooling ($\Delta T = 20$ °C, as the normal melting temperature of α-iPP is 165 °C), where the mobility of iPP molecular chains was high. The shear-induced oriented precursors may break down into point-like nuclei to induce homogeneous growth of iPP crystals.[40,50,60] While upon the shear flow field, polymer molecular chains and the tubular CNTs with one-dimensional geometrical structure are inclined to align parallel along the flow direction and then oriented polymer chains are absorbed on the surface of CNTs rather than relaxed, where the motion of extended iPP chains is restricted to form shish. As a consequence, CNTs display an amplification effect of shear on the orientation of iPP crystals.

Figure 5 depicts linear WAXD intensity profiles of iPP0 and iPP01 isothermally crystallized at 145 °C after step shear. Clearly, it takes a quite shorter time for both samples to engender the crystals compared with those two samples crystallized under quiescent condition (Figure 3). The coexistence of shear and CNTs takes the shortest time for inducing initial iPP crystallization, indicating that the coexistence of shear and CNTs further accelerates crystallization kinetics of iPP.

It is worthwhile to note that only α-crystals emerge in both sheared iPP0 and sheared iPP01 without any trace of β-crystals (Figure 5). It is well-known that the shear flow induces the oriented α-row-nuclei first, afterward β-crystals grow on the surface of the oriented α-crystals.[69,70] As mentioned above, α-row nuclei in sheared iPP0 may rapidly relax to point-like nuclei at a low degree of supercooling or at high Tc, thus losing the induction ability to form β-crystals.[69] In sheared iPP01, oriented crystals are clearly observed, where β-crystals are logically supposed to be present. Actually, β-crystals completely disappeared. It has been reported that CNTs act as α-crystal nucleating agent of iPP to induce the formation of α-crystals.[8,12,71] This may decrease the relative content of β-crystals at some extent. However, it seems not enough to completely eliminate β-crystals, due to the existence of oriented nuclei as well as the suitable temperature for β-crystal growth.[72] This will be further discussed later.

To get a comprehensive insight into the lamellar arrangement evolution of iPP under the coexistence of shear and CNTs, in situ SAXS measurement was carried out under the same thermo-mechanical history as in situ WAXD measurement (Figure 1a). Figure 6 presents a sequence of 2D-SAXS patterns of iPP0 and iPP01 isothermally crystallized at 145 °C after step shear. A pair of weak scattering maxima emerges immediately in the meridian upon cessation of flow and becomes stronger with time in both systems. There is no signal of equatorial streaks, which may be due to the small size of shish or the detection limit of SAXS.[32,66] For sheared iPP0, the 2D-SAXS patterns show obvious structural anisotropy, indicative of the lamellar arrangement with some preferred orientation, quite different from its 2D-WAXD result that the crystal structure seems to be homogeneously arranged (Figure 4 iPP0). This difference is attributed to the different detecting scales of WAXD and SAXS measurements.[73,74] Time-resolved linear SAXS profiles of iPP0 and iPP01 isothermally

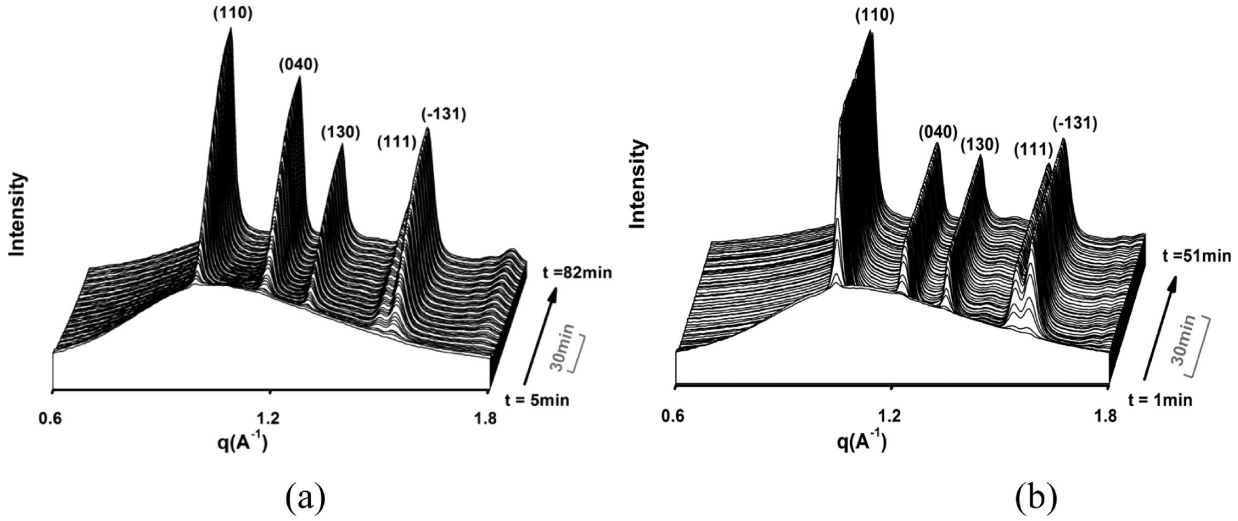

Figure 5. Linear WAXD intensity profiles of (a) iPP0 and (b) iPP01 crystallized at 145 °C after step shear as a function of scattering sector, q, of iPP melt, obtained from circularly integrated intensities of 2D-WAXD patterns in Figure 4.

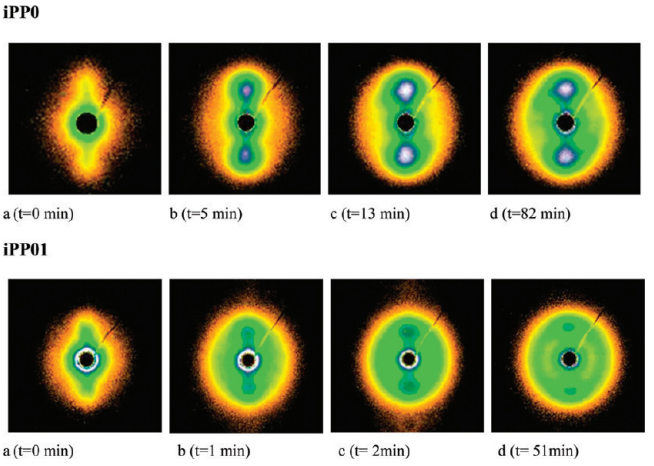

Figure 6. Selected 2D-SAXS patterns of iPP0 and iPP01 isothermally crystallized at 145 °C after step shear. The shear direction is vertical.

crystallized at 145 °C after step shear are illustrated in Figure 7. It is observed that scattering intensity of both samples gradually increases with time until it reaches a platform, corresponding to the completion of crystallization. Observing their time scales, the coexistence of shear and CNTs further enhance the crystallization kinetics of iPP, in consistence with above WAXD result.

To further reveal the combined effect of shear and CNTs on lamellar arrangement of iPP, the spacing between the adjacent lamellae (long period, L_B) in sheared iPP0 and sheared iPP01 is estimated and displayed as a function of time in Figure 8. In both sheared iPP0 and sheared iPP01, L_B decreases dramatically at the early stage of crystallization, indicating gradual generation of nucleation sites for new lamellar formation decreases the amorphous layer thickness. As crystals are mainly rearranged and perfected inside the original lamellae and the number of newly formed lamellae distinctly decreases during the progress of crystal growth, L_B gradually reaches a plateau value.[75,76] The similar phenomenon was observed by Fu et al. in iPP containing nanostructured polyhedral oligomeric silsesquioxane molecules (POSS) composites.[76] It is worth noting that L_B for sheared iPP01 is constantly less than that for sheared iPP0. The final value of L_B for sheared iPP01 (21.5 nm) is 3.1 nm low in comparison with sheared iPP0 (24.6 nm). The decrease of L_B is ascribed to the increased nucleation density under the coexistence of shear and CNTs.

Crystallization Kinetics. To further elucidate the combined effect of shear flow field and CNTs, we evaluated the crystallization kinetics of iPP in a quantitative way. The normalized relative crystallinity curves of quiescently crystallized and sheared iPP0 and iPP01 as a function of crystallization time are displayed in Figure 9. A typical sigmoidal evolution is seen in all four samples. Under the coexistence of shear and CNTs (Figure 9d), sheared iPP01 yields the shortest induction time (1 min) and completion time (51 min) among the four samples, while quiescently crystallized iPP0 yields the longest induction time (23 min) and completion time (248 min). The crystallization process of quiescently crystallized iPP01 (Figure 9b) seems to proceed constantly faster than sheared iPP0 (Figure 9c). Carefully identifying the inset picture in Figure 9, quiescently crystallized iPP01 displays a time lag of the induction time (6 min) but an accelerated crystallization rate compared to that of sheared iPP0 (5 min). This phenomenon indicates more time is needed for the start of CNTs-induced crystallization, but once crystallization starts, the crystallization kinetics is remarkably enhanced in terms of the great amount of CNT heterogeneous nuclei. The half crystallization time ($t_{1/2}$) of these four samples is listed in Table 1. $t_{1/2}$ of sheared iPP0 (29.5 min) is decreased to about 20% of the value (150.3 min) for quiescently crystallized iPP0. In other words, the crystallization rate of sheared iPP0 increases about 5 times of that of quiescently crystallized iPP0 accordingly which is ascribed to the increased homogeneous nuclei induced by shear. $t_{1/2}$ (20.7 min) of quiescently crystallized iPP01 is decreased by approximately 86% compared with that of quiescently crystallized iPP0 (150.3 min), i.e. the crystallization rate of quiescently crystallized iPP01 increases about 7 times of that of quiescently crystallized iPP0, testifying that CNTs are an effective nucleating agent for iPP crystallization.[7−11] CNTs, as a one-dimensional carbonaceous nanofiller, are reminiscent of a two-dimensional carbonaceous nanofiller, graphene nanosheet. It was found in our recent study that graphene nanosheets could also act as a nucleating agent for iPP crystallization as well, which reduced $t_{1/2}$ of iPP with 0.05 and

dx.doi.org/10.1021/ma201688p |*Macromolecules* 2011, 44, 8080–8092

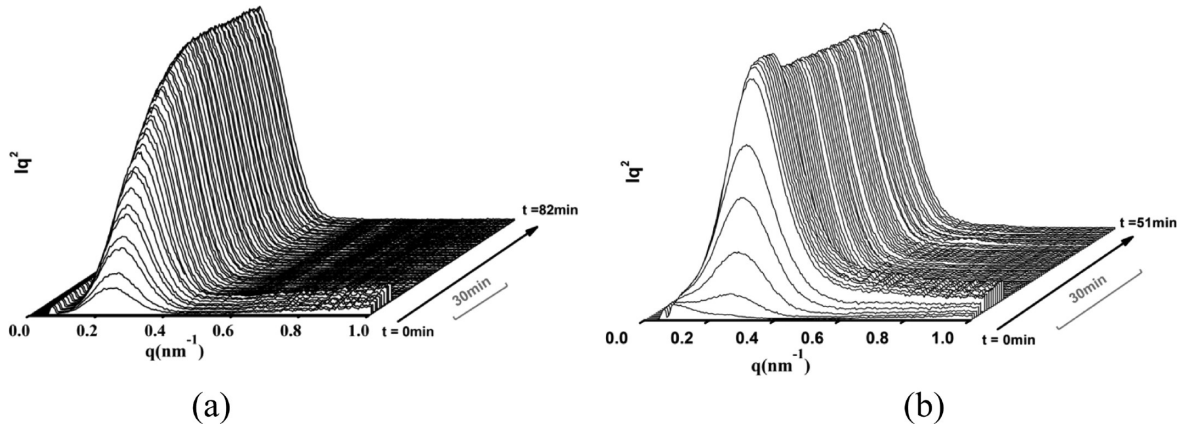

Figure 7. Linear SAXS intensity profiles of (a) iPP0 and (b) iPP01 crystallized at 145 °C after step shear as a function of scattering sector, q.

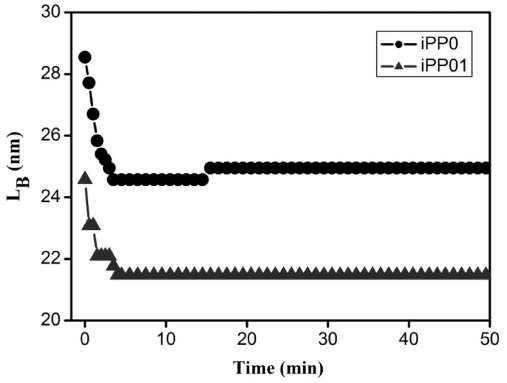

Figure 8. Time evolution profiles of the long periods as a function of crystallization time for iPP0 and iPP01 after step shear.

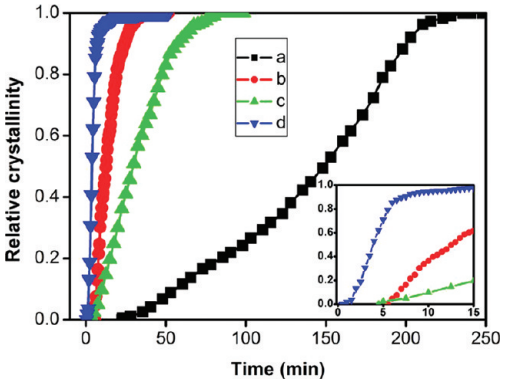

Figure 9. Normalized relative crystallinity in the iPP melt as a function of crystallization time, obtained from their linear WAXD curves in Figures 3 and 5. Key: (a) quiescently crystallized iPP0, (b) quiescently crystallized iPP01, (c) sheared iPP0, and (d) sheared iPP01. The inset picture magnifies the time axis at the beginning of crystallization.

0.1 wt % graphene nanosheets by just 50% compared with that of quiescently crystallized pure iPP.[50] It seems that CNTs are a kind of more effective nucleating agent for semicrystalline polymers than graphene nanosheets. This is also valid in the graphene nanosheets and CNTs-induced isothermal crystallization of strong polar semicrystalline polymer, poly(L-lactide) (PLLA).[77] Compared to graphene nanosheets, CNTs consist of larger

Table 1. Half Crystallization Time ($t_{1/2}$) of iPP0 and PP01 Isothermally Crystallized at 145 °C under Quiescent Condition and after Step Shear

	$t_{1/2}$	
	under quiescent condition (min)	under shear condition (min)
iPP0	150.3	29.5
iPP01	20.7	3.7

surface curvatures and more growth spacing, which are more favorable for nucleation and growth of semicrystalline polymers.[50,77]

Furthermore, the crystallization rate of sheared iPP01 (3.7 min) increases over 40 times compared to quiescently crystallized iPP0 (150.3 min). This increment is far beyond the simple addition of quiescently crystallized iPP01 and sheared iPP0 (just 35 times), indicating that the coexistence of shear and CNTs synergistically promotes the crystallization kinetics of iPP. It has been well established that shear could speed up crystallization kinetics by creating a quantity of oriented nuclei[7−11] while CNTs encourage crystallization kinetics by providing a great amount of nucleation sites.[18−22] When shear and CNTs are both present, it is logical to consider that the nuclei for growth of iPP crystals are additively originated from heterogeneous nucleating sites supplied by CNTs and oriented nuclei induced by shear. However, in the current case, just the simple addition of above two nucleus sources cannot reduce the $t_{1/2}$ to such a low level (3.7 min). There must be other nucleus sources for further enhanced crystallization kinetics. This will be discussed later.

Crystal Growth. Typical crystallization is a two-step process: (1) formation of stable nuclei (the nucleation stage) followed by (2) crystal growth characterized by the crystal growth rate (G).[78,79] At a given pressure (atmospheric pressure in the present case), G is set by the temperature. As the applied shear is quite weak (20 s^{-1}), the duration is short (5 s) and crystallization is performed under isothermal condition in this work, the crystal growth rate is fixed. The crystallization process is hence controlled by the nucleation stage. The modality of the nucleation is of technological importance since it not only contributes to the global crystallization rate, but also affects the crystal size distribution and crystal morphology and thereby the solid state properties of polymers. As aforementioned, the Avrami equation as a semiempirical

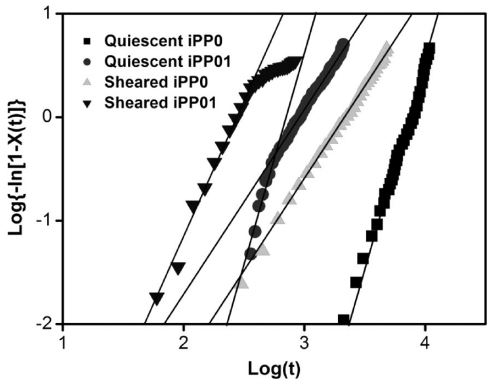

Figure 10. Avrami plots of the isothermal crystallization data of quiescent crystallized iPP0, quiescent crystallized iPP01, sheared iPP0, and sheared iPP01.

Table 2. Avrami Exponent *n* of iPP0 and iPP01 Isothermally Crystallized at 145°C under Quiescent Condition and after Step Shear

	Avrami exponent *n*	
	under quiescent condition	under shear
iPP0	4.00	1.82
iPP01	4.00/1.82	2.52

expression is widely used for isothermal crystallization process to reveal the nucleation mechanism and indirectly characterize the dimensionality of growth.[37−41,64] Here, the combination of shear and CNTs can synergistically accelerate crystallization kinetics of iPP, which are in close relation with the initial nucleation and successive crystal growth, thus Avrami equation is adopted as follows.[80−82]

$$X(t) = 1 - \exp(-kt^n) \quad (5)$$

Rewriting eq 5 in the following form:

$$\log\{-\ln[1 - X(t)]\} = n\log(t) + \log(k) \quad (6)$$

Here k is the bulk crystallization constant and n is the Avrami exponent. The normalized relative crystallinity $X(t)$ is derived from Figure 9. Avrami plots of quiescently crystallized and sheared iPP0 and iPP01 are present in Figure 10 and the Avrami exponent n is listed in Table 2. The Avrami exponent n of quiescently crystallized iPP0 (Figure 9a) is almost equal to 4.00. This is due to isotropic growth of iPP in the three-dimensional spherulite model as a result of thermal fluctuations in the melt.[52]

As for sheared iPP0 melt, the Avrami exponent n is equal to 1.82 (Table 2), corresponding to a two-dimensional lamellar growth geometry. This is basically consistent with the study on shear-induced iPP crystallization by Hsiao et al., where n was approximately equal to 2 and attributed to the sporadic nucleation of disk-like crystal geometry with diffusion controlled crystallization for pure iPP.[38,39] In our case when shear is imposed on iPP melt at a low supercooling, since shear-induced row-nuclei do not result from a thermodynamic process, they always tend to relax and break down into several small row-nuclei or point precursors which are capable of inducing two-dimensional growth of lamellar crystals (kebab) (see Figure 6).[40]

It is intriguing that there are two distinct growth stages in quiescently crystallized iPP01, where two linear fittings are needed to describe the crystal growth, as shown in Figure 10. First, Avrami exponent n is approximately equal to 4.00, indicative of initial crystals growth in three-dimensional spherulite model, and then changes to a lower value, only 1.82, where two-dimensional lamellar growth pattern dominates. Two Avrami exponent constants mean two different nucleation and crystal growth processes. At the early stage of crystallization, a great amount of heterogeneous nuclei provided by CNTs surface and spontaneous homogeneous nuclei derived from thermal fluctuations both exist, but only homogeneous nuclei first induce crystallization in the three-dimensional spherulitic growth, resembling the growth geometry of quiescently crystallized iPP0. Later, heterogeneous nuclei take effect to induce two-dimensional lamellar growth, which, to an extent, is like shear-induced lamellar growth (sheared iPP0). This is probably because crystal growth originated from heterogeneous nuclei on CNT surface is controlled by the process of absorption of iPP molecular chains to the surface of CNTs and successive crystal epitaxial growth, which may take longer time than crystal growth generated by spontaneous homogeneous nuclei. Therefore, few spontaneous homogeneous nuclei first initiate few spherulites and then heterogeneous nuclei dominate to markedly engender the formation of lamellae. This two-stage growth has never been reported in the previous studies on CNTs-induced polymer crystallization, which may intimately related to the CNT concentration, dispersion state, aspect ratio and crystallization conditions, etc.[7−9,11,17] The dimensionality of CNTs-induced crystal growth evaluated by Avrami exponent has been discussed controversially. Winey et al. indicated that the crystal dimensionality was reduced from spherulitic to disk-shaped, due to n approximately equal to 1.6 for PE composites in the presence of 1 wt % SWNTs.[11] Kaminsky et al. pointed out in the CNTs/iPP system that the dimensionality changed from a disk-like growth with instantaneous nucleation to a random nucleation or from a rod-like to a more disk-like growth (with random nucleation), with n ranging from 2 to 2.8.[17] Others argued after the addition of CNTs to iPP that n close to 3 was practically unchanged compared to pure iPP, implying a three-dimensional heterogeneous crystal growth.[7−9] Our result is basically in line with the results of Winey et al.[11] and Kaminsky et al.,[17] but a main difference exists that only 0.1 wt % CNT is quite low compared to their loadings. Moreover, van Mele and Loos et al. visually observed an iPP transcrystalline layer highly oriented around the nucleating CNTs in CNTs/iPP composites prepared by latex technology, which strongly supports our results.[67,71]

Under the coexistence of shear and CNTs (sheared iPP01 in Figure 10), Avrami exponent n surprisingly increases to 2.52, suggestive of mixed growth geometry of two-dimensional lamellar growth and three-dimensional spherulitic growth. This mixed growth geometry is much involved with nucleation and subsequent crystal growth under the interaction between shear and CNTs. Details will be discussed later. Additionally, the divergence of the curve of sheared iPP01 is ascribed to subsequent secondary crystallization with gradual crystal growth perfection, which usually happens after the fast primary crystallization.

Crystal Orientation. Flow imposes some orientation on the crystals, which is an important factor to influence the final properties. In order to reveal the combined effect of shear and CNTs on iPP crystal orientation, degree of orientation of iPP0 and iPP01 after step shear as a function of time under isothermal crystallization is present in Figure 11. It can be seen that both curves

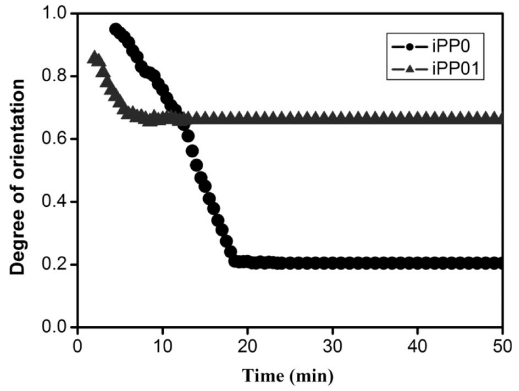

Figure 11. Degree of orientation as a function of crystallization time for iPP0 and iPP01 isothermally crystallized at 145 °C after step shear.

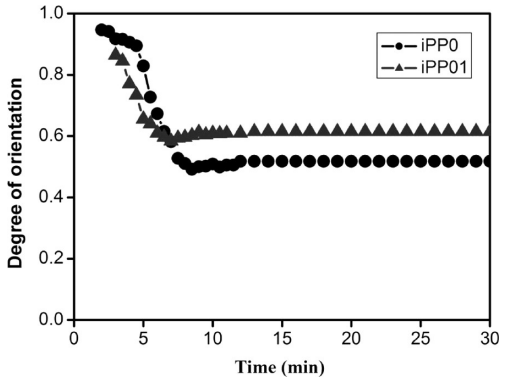

Figure 12. Degree of orientation as a function of crystallization time for iPP0 and iPP01 nonisothermally crystallized from 150 °C after step shear.

display an L-type, where there is a high degree of orientation at the beginning, whereafter gradually a decreased value, and a constant level after a critical time. This is due to the initial formation of highly oriented crystals and subsequent crystal growth without any preferred orientation.[83]

For sheared iPP0, the degree of orientation of initial crystals is about 0.95, and then gradually attenuates to about 0.20. It is believed that after shear cessation the stability of the oriented morphology is a compromise between crystallization and chain relaxation.[84] After the shear impulse, few oriented crystals with a high degree of orientation emerge, based on the remaining row-nuclei. Nevertheless, under the high crystallization temperature (low supercooling) most of the oriented molecular chains which do not result from a thermodynamic process are relaxed to form point-like nuclei rather than persisting row-nuclei, thus isotropic growth is dominant in the later crystallization process and final crystals show a quite low degree of orientation, which basically can be ignored (Figure 4).

It is interesting to note that sheared iPP01 exhibit a lower degree of orientation (0.86) in the early crystallization stage but a higher degree of orientation (0.63) at the later crystallization stage, compared to sheared iPP0. The intrinsic properties of pure iPP melt may be altered since the presence of CNTs makes the response of CNTs/iPP nanocomposites to shear complicated.

DISCUSSION

Under the coexistence of shear and CNTs (sheared iPP01 sample), interaction between shear and CNTs inevitably exists, which demonstrates a significant influence on the crystallization of iPP, such as evolution of crystal orientation, crystallization kinetics and crystal growth, and even polymorphism of iPP.

After step shear, the presence of CNTs in iPP01 resulted in apparent crystal orientation in all 2D-WAXD patterns while iPP0 only showed isotropic diffraction rings (Figure 4). The degree of orientation in sheared iPP0 and sheared iPP01 during the whole isothermal crystallization showed that sheared iPP01 exhibited a lower degree of orientation (0.86) in the early crystallization stage but a higher (0.63) at the later crystallization stage, compared to sheared iPP0, which has never been noticed by the previous studies.[57,58,62,63] CNTs that interpenetrated the polymer matrix created additional and large contributions to nanocomposite viscoelasticity (see the rheological data in the Supporting Information).[85] When the shear flow was imposed on the CNTs/iPP melt, the increased viscoelasticity consumed part of the shear force that was supposed to orient the molecular chains, leading to lower orientation of molecular chains in the CNTs/iPP melt, compared to that in the sheared pure iPP melt at the commencement, namely, the presence of CNTs suppressed the initial formation of highly oriented molecular chains, eventually lowering the initial degree of orientation. The reasons for higher crystal orientation in resultant sheared iPP01 were explained as follows. Additives (nucleating agents, fibers, particles, and CNTs etc.) generally served as point nuclei on which polymer molecular chains can be absorbed and subsequently be stretched along the flow field to form thread-like precursors.[55,56] The precursors can be stabilized by the adsorption of additives surfaces[57,58] or the network interconnected by additives[59] to form oriented structures other than relaxed. Therefore, as for filled polymers crystallized after shear flow, the orientation is usually enhanced in comparison to pure polymers,[49,50,59−61] especially in the case of CNTs/polymer nanocomposite system due to well-dispersed, one-dimensional and anisotropic characteristics of CNTs.[57,58,62,63] What needs to be pointed out is that, in our case, the oriented precursors were stabilized by CNT surface adsorption instead of CNT network confinement, concluded from our rheological data in Supporting Information where there is no sign of the formation of CNT network at such low CNT content (0.1 wt %). In a word, initial suppression of the orientation of molecular chains and subsequent stabilization of oriented molecular chains are ascribed to interaction between shear and CNTs. As aforementioned, polymer molecular chains exhibited high mobility in low supercooling, which are not favorable for persisting the oriented molecular chains after step shear. In order to avoid the influence of supercooling and further testify the effect of interaction on evolution of crystal orientation under isothermal crystallization, the evolution of crystal orientation in sheared iPP0 and sheared iPP01 melt under nonisothermal crystallization was also characterized by 2D-WAXD following the procedure in Figure 1b, as shown in Figure 12. It was also observed that sheared iPP01 yielded lower (0.87) initial and higher final degree of orientation (0.60) in comparison to sheared iPP0. We believe that this influence of interaction between shear and CNTs on evolution of crystal orientation can be generally applied to crystallization of polymer composite system with various kinds of nanoscale additives after shear.

For sheared iPP01, the crystallization kinetics was further accelerated by decreasing $t_{1/2}$ (3.7 min) to about just 2% of that of quiescently crystallized iPP0 ($t_{1/2}$ = 150.3 min), namely, increasing the crystallization rate over 40 times compared to quiescently

crystallized iPP0 (see Figure 9 and Table 1). This increment was more significant than the simple addition of quiescently crystallized iPP01 and sheared iPP0 (just 35 times), indicating that the coexistence of shear and CNTs synergistically promoted the crystallization kinetics of iPP. Simple addition of nuclei originated from shear and CNTs cannot decrease the crystallization kinetics so immensely, there must be other nucleus sources for iPP crystallization. Following the point of view in our previous study on shear-induced iPP crystallization with β-nucleating agent, interplay, which were present between shear and β-nucleating agent, were able to create extra nuclei for crystal growth.[52] Accordingly, extra nuclei can be also created by the interaction between shear and CNTs since CNTs as α-nucleating agent acted like β-nucleating agent particles. These extra nuclei further enhanced the crystallization kinetics. What is more, these extra nuclei gave rise to the more pronounced decrease of L_B in sheared iPP01 compared to sheared iPP0 (Figure 8).

Apart from further accelerating crystallization kinetics, extra nuclei were capable of altering the crystal growth of sheared iPP01. As observed in Figure 10, Avrami exponent n surprisingly increased to 2.52, implying mixed growth geometry, i.e. two-dimensional lamellar growth and three-dimensional spherulitic growth. We considered the shear-induced oriented nuclei and CNTs-induced heterogeneous nuclei accounted for the two-dimensional lamellar growth, which has been proved by their Avrami exponents approximately equal to 1.82 (Figure 10 and Table 2). However, the extra nuclei created by interplay between shear and CNTs were responsible for three-dimensional spherulitic growth. Here are the reasons. It is reported that n value is connected to the number of growth points in crystal nuclei; in other words, the more the growth points are, the larger the n value.[86] The spherulites are formed by the growth of branches of lamellae in an unsymmetrical mode, relying on growth points of branching sites on the lamellae. The greater branching sites and the more growth points bring out a larger Avrami exponent n.[87] In our case, CNTs stabilized the oriented molecular chains induced by shear through surface absorption. The surface absorption made the oriented molecular chains difficult to relax back to random molecular chains. Some of these oriented molecular chains form oriented nuclei for lamellar growth. Others still persisting low entropy became active growth points (extra nuclei) of branching sites on the lamellae to generate spherulitic growth. Therefore, under coexistence of shear and CNTs, iPP crystals grow in two-dimensional lamellar and three-dimensional spherulitic growth manners. This is quite different from the study on PBT melt containing CNTs performed by Mago et al.,[64] in which unexpectedly and significantly high (6.5−8.0) values of the Avrami exponent n were calculated by an Avrami-type equation for the normalized storage modulus. They believed the underlying reason for the higher values of the Avrami exponent was associated with shear-induced crystallization versus those determined under quiescent conditions.

Another interesting phenomenon in Figure 4 was needed to note that the complete absence of β-crystals in both sheared iPP0 and iPP01 samples. It is easy to understand the absence of β-crystals in sheared iPP0, since shear-induced row-nuclei relaxed into point-like nuclei and then lost the ability to induce β-crystals at high temperature (Figures 4 and 5). The similar phenomenon has been reported by Varga et al. They indicated that by pulling the glass fiber in iPP melt α-row-nuclei could be developed, whose surface could induce the growth of β-crystals leading to the formation of cylindrites. However, the capability of α-row-nuclei to induce β-crystals was lost by repeatedly crystallizing and melting.[69]

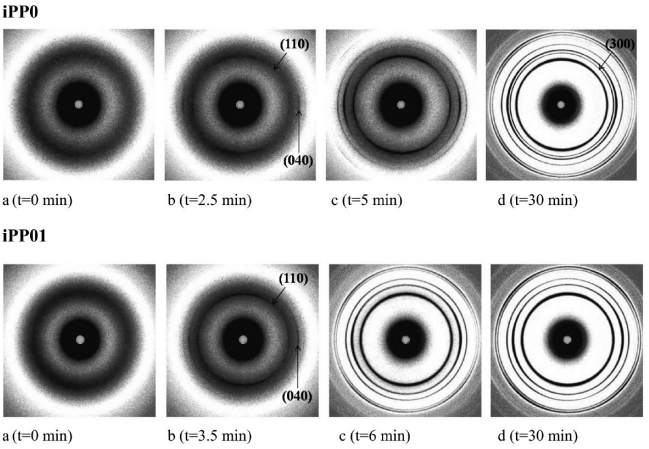

Figure 13. Selected 2D-WXAD patterns showing the crystal growth process of iPP nonisothermally crystallized from 150 °C after step shear.

In the case of sheared iPP01, according to above logic, oriented crystals were clearly observed and thus β-crystals were supposed to be present. Unexpectedly, β-crystals were completely absent in sheared iPP01. Normally, CNTs act as α-crystal nucleating agent of iPP to induce α-crystals,[8,12,71] which may just decrease the relative content of β-crystals, but cannot completely eliminate β-crystals, due to the existence of oriented nuclei as well as the suitable temperature for β-crystal growth.[69]

Low supercooling may accelerate relaxation of oriented row-nuclei, which is disadvantageous to the formation of β-crystals. To further reveal the reasons for the complete absence of β-crystals under the coexistence of shear and CNTs on the basis of excluding the effect of supercooling, a nonisothermal crystallization experiment as depicted in Figure 1b was carried out. A series of 2D-WAXD patterns of sheared iPP0 and sheared iPP01 are shown in Figure 13. In sheared iPP0, obvious arc-like diffraction feature along the meridian from oriented α-crystals is observed in the whole crystallization process, demonstrating that shear-induced row-nuclei are retained and further develop into oriented crystals. The integrated linear WAXD profiles are shown in Figure 14a. It is seen that a fair amount of β-crystals emerges in sheared iPP0. This evidence definitively confirms that row-nuclei persisted by the cooling treatment are capable of inducing β-crystals. Although shear-induced row-nuclei are also formed at the initial period of crystallization and successively oriented crystals grew on these nuclei in sheared iPP01 (Figure 13), no β-crystals emerge in Figure 14b. Besides strong α-nucleation efficiency of CNTs, it is believed that extra nuclei, which was believed to be α-nuclei because interaction between shear and CNTs can greatly lower the entropy of the system, favoring the formation of α-nuclei, should be responsible for the complete inexistence of β-crystals. Hence, the extra nuclei as well as α-nuclei from CNTs encouraged the formation of α-crystals, resulting in complete inexistence of β-crystals.

The iPP crystallization process under the coexistence of shear and CNTs is schematically illustrated in Figure 15. Before the application of shear, CNTs were randomly dispersed in the matrix of coiled iPP molecular chains (Figure 15a). During shear, both CNTs and iPP chains tended to align along the flow direction (Figure 15b). Subsequently, due to the absorption of CNTs, the relaxation of the molecular chains in the surrounding of CNTs was hindered and part of oriented chains evolved into shish and other random molecular chains started to epitaxially grow on CNT

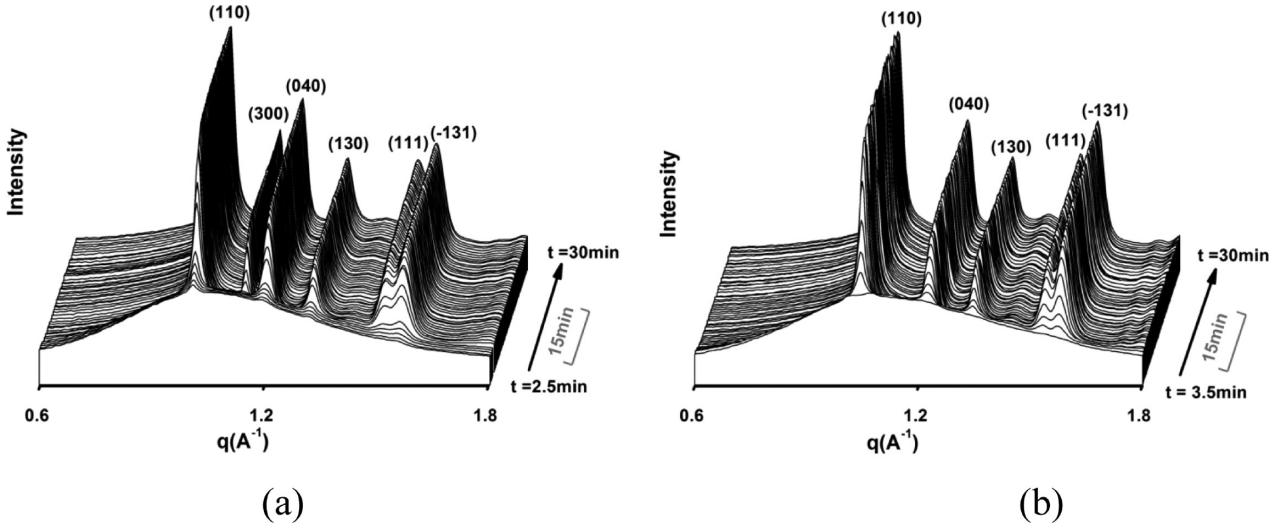

Figure 14. Linear WAXD intensity profiles of (a) iPP0 and (b) iPP01 after step shear as a function of scattering sector, q, of iPP melt, obtained from circularly integrated intensities of 2D-WAXD patterns in Figure 13.

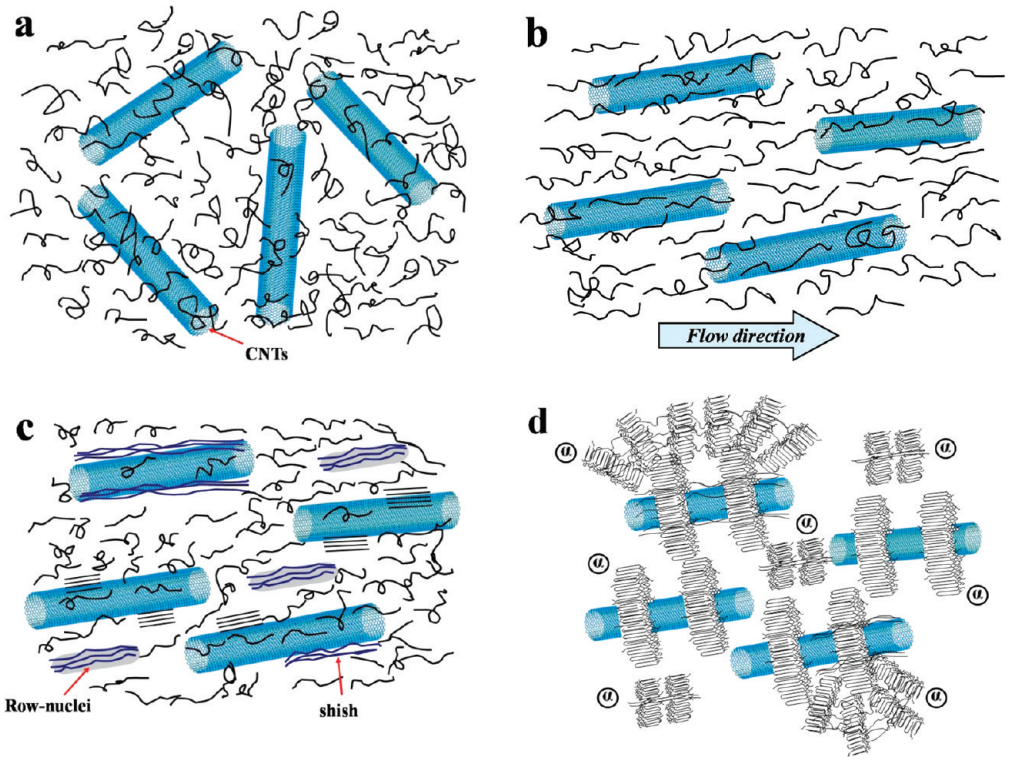

Figure 15. Schematic diagrams of the morphological development of CNTs/iPP nanocomposites with before and after shear. Key (a) randomly dispersed CNTs and coiled iPP molecular chains before shear, (b) orientation of CNTs and iPP molecular chains just after shear, (c) the formation of shish on CNT surface and row-nuclei in the matrix and primary epitaxial growth of random molecular chains on CNT surface, and (d) subsequent lamellar growth originated by CNT surface, shish on CNT surface, and shear-induced row-nuclei in the matrix, with spherultic growth based on extra nuclei from the interaction between shear and CNTs.

surface, while in the melt some of oriented molecular chains formed row-nuclei (Figure 15c). Eventually, lamellar growth was induced by CNT surface, shish on CNT surface and shear-induced row-nuclei, and then spherultic growth was engendered by extra nuclei generated by the interaction between shear and CNTs (Figure 15d). Because of the existence of extra nuclei created by interaction between shear and CNTs, CNTs/iPP nanocomposites exhibited a synergistic effect on accelerating crystallization kinetics of iPP and the crystal growth of iPP was in the mode of mixed two-dimensional lamellar and three-dimensional spherulitic growth. In addition to α-crystal nucleation ability of CNTs, β-crystals completely disappeared.

CONCLUSIONS

The crystallization of iPP under the coexistence of shear flow and CNTs was investigated by in situ synchrotron X-ray scattering techniques (WAXD and SAXS). Crystal orientation, crystallization kinetics, crystal growth and polymorphism of iPP were significantly influenced by the inevitable interaction between shear flow and CNTs, which generated that formation of extra nuclei.

Degree of orientation of sheared CNTs/iPP nanocomposites exhibited lower level at the early period of crystallization but achieved a higher plateau at the end compared to that of sheared pure iPP. Just when the shear was applied to CNTs/iPP melt, initial orientation of molecular chains was suppressed due to increased viscoelasticity of iPP melt caused by the presence of CNTs, giving rise to lower crystal orientation than that of sheared pure iPP. Once oriented molecular chains were formed, CNTs took effect to stabilize the oriented molecular chains and endow the crystals with higher resultant crystal orientation in comparison to that of sheared pure iPP.

The crystallization rate of sheared CNTs/iPP nanocomposites was increased about 40 times, compared to that of quiescently crystallized pure iPP, exceeding the simple addition of quiescently crystallized CNTs/iPP nanocomposites and sheared pure iPP (just 35 times). This illustrates the coexistence of shear and CNTs synergistically promoted the crystallization kinetics of sheared CNTs/iPP nanocomposites since extra nuclei created by interaction between shear flow and CNTs accounted for the further accelerated crystallization rate.

Analyzing the Avrami exponent n, the crystal growth geometry of sheared CNTs/iPP nanocomposites altered from three-dimensional sphrulitic growth of quiescently crystallized pure iPP ($n \approx 4.00$), two-dimensional lamellar growth of sheared pure iPP ($n \approx 1.82$), and quiescently crystallized CNTs/iPP nanocomposites ($n \approx 1.82$) to mixed three-dimensional sphrulitic growth and two-dimensional lamellar growth ($n \approx 2.52$), as the extra nuclei acted as active growth points of branching sites on the lamellae to generate spherulitic growth. Moreover, extra nuclei as well as α-nuclei from CNTs encouraged the formation of α-crystals, resulting in complete absence of β-crystals. As for polymer composites under practical processing condition, the interaction between shear flow field and additives is inevitable and its effect on crystallization behavior of polymer should be fully considered in order to obtain high-performance polymer composites.

ASSOCIATED CONTENT

Supporting Information. DSC curves of iPP0 and iPP01, complex viscosity and storage modulus of iPP0 and iPP01, and observation of CNTs dispersion in iPP matrix. This material is available free of charge via the Internet at http://pubs.acs.org/.

AUTHOR INFORMATION

Corresponding Author

*E-mail: (Z.-M.L.) zmli@scu.edu.cn; (B.S.H.) bhsiao@notes.cc.sunysb.edu.

ACKNOWLEDGMENT

The authors are indebted to Dr. Lixia Rong and Jie Zhu from Synchrotron Light Source, Brookhaven National Laboratory (USA) for their help of in situ synchrotron X-ray scattering measurement. The Chinese team expresses thanks for the financial support by the National Outstanding Youth Foundation of China (Grant No. 50925311) and the State Key Program of National Natural Science of China (Grant No. 51033004, 20876099), and the US team expresses thanks for financial support by the National Science Foundation of the US (DMR-0906512).

REFERENCES

(1) Spitalsky, Z.; Tasis, D.; Papagelis, K.; Galiotis, C. *Prog. Polym. Sci.* **2010**, *35*, 357–401.
(2) Li, Y. L.; Kinloch, I. A.; Windle, A. H. *Science* **2004**, *304*, 276–278.
(3) Tans, S. J.; Verschueren, A. R. M.; Dekker, C. *Nature* **1998**, *393*, 49–52.
(4) Odom, T. W.; Huang, J. L.; Kim, P.; Lieber, C. M. *Nature* **1998**, *391*, 62–64.
(5) Treacy, M. M. J.; Ebbesen, T. W.; Gibson, J. M. *Nature* **1996**, *381*, 678–680.
(6) Marco, C.; Naffakh, M.; Gomez, M. A.; Santoro, G.; Ellis, G. *Polym. Compos.* **2011**, *32*, 324–333.
(7) Grady, B. P.; Pompeo, F.; Shambaugh, R. L.; Resasco, D. E. *J. Phys. Chem. B* **2002**, *106*, 5852–5858.
(8) Bhattacharyya, A. R.; Sreekumar, T. V.; Liu, T.; Kumar, S.; Ericson, L. M.; Hauge, R. H.; Smalley, R. E. *Polymer* **2003**, *44*, 2373–2377.
(9) Xu, D. H.; Wang, Z. G. *Polymer* **2008**, *49*, 330–338.
(10) Anoop Anand, K.; Agarwal, U. S.; Joseph, R. *Polymer* **2006**, *47*, 3976–3980.
(11) Haggenmueller, R.; Fischer, J. E.; Winey, K. I. *Macromolecules* **2006**, *39*, 2964–2971.
(12) Assouline, E.; Lustiger, A.; Barber, A. H.; Cooper, C. A.; Klein, E.; Wachtel, E.; Wagner, H. D. *J. Polym. Sci., Part B: Polym. Phys.* **2003**, *41*, 520–527.
(13) Li, L. Y.; Li, C. Y.; Ni, C. Y. *J. Am. Chem. Soc.* **2006**, *128*, 1692–1699.
(14) Li, C. Y.; Li, L. Y.; Cai, W. W.; Kodjie, S. L.; Tenneti, K. K. *Adv. Mater.* **2005**, *17*, 1198–1202.
(15) Yang, J. H.; Wang, C. Y.; Wang, K.; Zhang, Q.; Chen, F.; Du, R. N.; Fu, Q. *Macromolecules* **2009**, *42*, 7016–7023.
(16) Yang, J. H.; Wang, K.; Deng, H.; Chen, F.; Fu, Q. *Polymer* **2010**, *51*, 774–782.
(17) Funck, A.; Kaminsky, W. *Compos. Sci. Technol.* **2007**, *67*, 906–915.
(18) Kumaraswamy, G.; Issaian, A. M.; Kornfield, J. A. *Macromolecules* **1999**, *32*, 7537–7547.
(19) Kumaraswamy, G.; Verma, R. K.; Issaian, A. M.; Wang, P.; Kornfield, J. A.; Yeh, F.; Hsiao, B. S.; Olley, R. H. *Polymer* **2000**, *41*, 8931–8940.
(20) Kumaraswamy, G.; Kornfield, J. A.; Yeh, F. J.; Hsiao, B. S. *Macromolecules* **2002**, *35*, 1762–1769.
(21) Housmans, J. W.; Steenbakkers, R. J. A.; Roozemond, P. C.; Peters, G. W. M.; Meijer, H. E. H. *Macromolecules* **2009**, *42*, 5728–5740.
(22) Pantani, R.; Coccorullo, I.; Volpe, V.; Titomanlio, G. *Macromolecules* **2010**, *43*, 9030–9038.
(23) Janeschitz-Kriegl, H.; Ratajski, E.; Stadlbauer, M. *Rheol. Acta* **2003**, *42*, 355–364.
(24) Zhu, P. W.; Edward, G. *Polymer* **2004**, *45*, 2603–2613.
(25) Hsiao, B. S.; Yang, L.; Somani, R. H.; Avila-Orta, C. A.; Zhu, L. *Phys. Rev. Lett.* **2005**, 94.
(26) Somani, R. H.; Yang, L.; Zhu, L.; Hsiao, B. S. *Polymer* **2005**, *46*, 8587–8623.
(27) Cao, W.; Wang, K.; Zhang, Q.; Du, R. N.; Fu, Q. *Polymer* **2006**, *47*, 6857–6867.
(28) Chan, N. Y.; Chen, M.; Hao, X. T.; Smith, T. A.; Dunstan, D. E. *J. Phys. Chem. Lett.* **2010**, *1*, 1912–1916.
(29) Zhu, J. X.; Li, M.; Rogers, R.; Meyer, W.; Ottewill, R. H.; Russell, W. B.; Chaikin, P. M. *Nature* **1997**, *387*, 883–885.
(30) Lellinger, D.; Foudas, G.; Alig, I. *Polymer* **2003**, *44*, 5759–5769.
(31) de Gennes, P. G. *J. Chem. Phys.* **1970**, *60*, 5030–5042.
(32) Yang, L.; Somani, R. H.; Sics, I.; Hsiao, B. S.; Kolb, R.; Fruitwala, H.; Ong, C. *Macromolecules* **2004**, *37*, 4845–4859.

(33) Somani, R. H.; Hsiao, B. S.; Nogales, A.; Srinivas, S.; Tsou, A. H.; Sics, I.; Balta-Calleja, F. J.; Ezquerra, T. A. *Macromolecules* **2000**, *33*, 9385–9394.
(34) Kalay, G.; Bevis, M. J. *J. Polym. Sci., Part B: Polym. Phys.* **1997**, *35*, 241–263.
(35) Housmans, J. W.; Gahleitner, M.; Peters, G. W. M.; Meijer, H. E. H. *Polymer* **2009**, *50*, 2304–2319.
(36) Kalay, G.; Sousa, R. A.; Reis, R. L.; Cunha, A. M.; Bevis, M. J. *J. Appl. Polym. Sci.* **1999**, *73*, 2473–2483.
(37) Masubuchi, Y.; Watanabe, K.; Nagatake, W.; Takimoto, J. I.; Koyama, K. *Polymer* **2001**, *42*, 5023–5027.
(38) Agarwal, P. K.; Somani, R. H.; Weng, W. Q.; Mehta, A.; Yang, L.; Ran, S. F.; Liu, L. Z.; Hsiao, B. S. *Macromolecules* **2003**, *36*, 5226–5235.
(39) Avila-Orta, C. A.; Burger, C.; Somani, R.; Yang, L.; Marom, G.; Medellin-Rodriguez, F. J.; Hsiao, B. S. *Polymer* **2005**, *46*, 8859–8871.
(40) Li, L. B.; de Jeu, W. H. *Macromolecules* **2004**, *37*, 5646–5652.
(41) Madbouly, S. A.; Ougizawa, T. *J. Macromol. Sci., Phys.* **2003**, *B42*, 269–281.
(42) Chen, Y. H.; Zhong, G. J.; Wang, Y.; Li, Z. M.; Li, L. B. *Macromolecules* **2009**, *42*, 4343–4348.
(43) Zhang, G.; Karger-Kocsis, J.; Zou, J. *Carbon* **2010**, *48*, 4289–4300.
(44) Corte, L.; Beaume, F.; Leibler, L. *Polymer* **2005**, *46*, 2748–2757.
(45) Cao, Q.; Kim, H. S.; Pimparkar, N.; Kulkarni, J. P.; Wang, C. J.; Shim, M.; Roy, K.; Alam, M. A.; Rogers, J. A. *Nature* **2008**, *454*, 495–U4.
(46) Lagasse, R. R.; Maxwell, B. *Polym. Eng. Sci.* **1976**, *16*, 189–199.
(47) Naudy, S.; David, L.; Rochas, C.; Fulchiron, R. *Polymer* **2007**, *48*, 3273–3285.
(48) D'Haese, M.; Van Puyvelde, P.; Langouche, F. *Macromolecules* **2010**, *43*, 2933–2941.
(49) Larin, B.; Avila-Orta, C. A.; Somani, R. H.; Hsiao, B. S.; Marom, G. *Polymer* **2008**, *49*, 295–302.
(50) Xu, J. Z.; Chen, C.; Wang, Y.; Tang, H.; Li, Z. M.; Hsiao, B. S. *Macromolecules* **2011**, *44*, 2808–2818.
(51) Byelov, D.; Panine, P.; Remerie, K.; Biemond, E.; Alfonso, G. C.; de Jeu, W. H. *Polymer* **2008**, *49*, 3076–3083.
(52) Chen, Y. H.; Mao, Y. M.; Li, Z. M.; Hsiao, B. S. *Macromolecules* **2010**, *43*, 6760–6771.
(53) Nowacki, R.; Monasse, B.; Piorkowska, E.; Galeski, A.; Haudin, J. M. *Polymer* **2004**, *45*, 4877–4892.
(54) Hwang, W. R.; Peters, G. W. M.; Hulsen, M. A.; Meijer, H. E. H. *Macromolecules* **2006**, *39*, 8389–8398.
(55) Jerschow, P.; Janeschitz-Kriegl, H. *Int. Polym. Process* **1997**, *12*, 72–77.
(56) Janeschitz-Kriegl, H. *Macromolecules* **2006**, *39*, 4448–4454.
(57) Garcia-Gutierrez, M. C.; Hernandez, J. J.; Nogales, A.; Panine, P.; Rueda, D. R.; Ezquerra, T. A. *Macromolecules* **2007**, *41*, 844–851.
(58) Patil, N.; Balzano, L.; Portale, G.; Rastogi, S. *Carbon* **2010**, *48*, 4116–4128.
(59) Zhong, G. J.; Li, L. B.; Mendes, E.; Byelov, D.; Fu, Q.; Li, Z. M. *Macromolecules* **2006**, *39*, 6771–6775.
(60) Nogales, A.; Mitchell, G. R. R.; Vaughan, A. S. *Macromolecules* **2003**, *36*, 4898–4906.
(61) Larin, B.; Lyashenko, T.; Harel, H.; Marom, G. *Compos. Sci. Technol.* **2011**, *71*, 177–182.
(62) Patil, N.; Balzano, L.; Portale, G.; Rastogi, S. *Macromol. Chem. Phys.* **2009**, *210*, 2174–2187.
(63) Patil, N.; Balzano, L.; Portale, G.; Rastogi, S. *Macromolecules* **2010**, *43*, 6749–6759.
(64) Mago, G.; Fisher, F. T.; Kalyon, D. M. *Macromolecules* **2008**, *41*, 8103–8113.
(65) Krache, R.; Benavente, R.; Lopez-Majada, J. M.; Perena, J. M.; Cerrada, M. L.; Perez, E. *Macromolecules* **2007**, *40*, 6871–6878.
(66) Somani, R. H.; Yang, L.; Hsiao, B. S.; Sun, T.; Pogodina, N. V.; Lustiger, A. *Macromolecules* **2005**, *38*, 1244–1255.
(67) Miltner, H. E.; Grossiord, N.; Lu, K. B.; Loos, J.; Koning, C. E.; Van Mele, B. *Macromolecules* **2008**, *41*, 5753–5762.
(68) Azzurri, F.; Alfonso, G. C. *Macromolecules* **2005**, *38*, 1723–1728.
(69) Varga, J.; Karger-Kocsis, J. *J. Polym. Sci., Part B: Polym. Phys.* **1996**, *34*, 657–670.
(70) Somani, R. H.; Hsiao, B. S.; Nogales, A.; Fruitwala, H.; Srinivas, S.; Tsou, A. H. *Macromolecules* **2001**, *34*, 5902–5909.
(71) Lu, K. B.; Grossiord, N.; Koning, C. E.; Miltner, H. E.; van Mele, B.; Loos, J. *Macromolecules* **2008**, *41*, 8081–8085.
(72) Varga, J. *J. Mater. Sci.* **1992**, *27*, 2557–2579.
(73) Wang, Z. G.; Hsiao, B. S.; Sirota, E. B.; Agarwal, P.; Srinivas, S. *Macromolecules* **2000**, *33*, 978–989.
(74) Somani, R. H.; Yang, L.; Hsiao, B. S.; Agarwal, P. K.; Fruitwala, H. A.; Tsou, A. H. *Macromolecules* **2002**, *35*, 9096–9104.
(75) Wen, H. Y.; Jiang, S. C.; Men, Y. F.; Zhang, X. Q.; An, L. J.; Wu, Z. H.; Okuda, H. *Macromol. Chem. Phys.* **2008**, *209*, 1721–1729.
(76) Fu, B. X.; Yang, L.; Somani, R. H.; Zong, S. X.; Hsiao, B. S.; Phillips, S.; Blanski, R.; Ruth, P. *J. Polym. Sci., Part B: Polym. Phys.* **2001**, *39*, 2727–2739.
(77) Xu, J. Z.; Chen, T.; Yang, C. L.; Li, Z. M.; Mao, Y. M.; Zeng, B. Q.; Hsiao, B. S. *Macromolecules* **2010**, *43*, 5000–5008.
(78) Lauritzen, J. I.; Hoffman, J. D. *J. Res. Natl. Bur. Stand. U.S.A.* **1960**, *64A*, 73–102.
(79) Hoffman, J. D.; Lauritzen, J. I. *J. Res. Natl. Bur. Stand. U.S.A.* **1961**, *65A*, 297–336.
(80) Avrami, M. *J. Chem. Phys.* **1939**, *7*, 1103–1112.
(81) Avrami, M. *J. Chem. Phys.* **1940**, *8*, 212–224.
(82) Avrami, M. *J. Chem. Phys.* **1941**, 177–184.
(83) Mao, Y. M.; Burger, C.; Zuo, F.; Hsiao, B. S.; Mehta, A.; Mitchell, C.; Tsou, A. H. *Macromolecules* **2011**, *44*, 558–565.
(84) Gutierrez, M. C. G.; Alfonso, G. C.; Riekel, C.; Azzurri, F. *Macromolecules* **2004**, *37*, 478–485.
(85) Kharchenko, S. B.; Douglas, J. F.; Obrzut, J.; Grulke, E. A.; Migler, K. B. *Nat. Mater.* **2004**, *3*, 564–568.
(86) Bian, J.; Ye, S. R.; Feng, L. X. *J. Polym. Sci., Part B: Polym. Phys.* **2003**, *41*, 2135–2144.
(87) Naffakh, M.; Marco, C.; Gómez-Fatou, M. A. *J. Phys. Chem. B* **2011**, *115*, 2248–2255.